Check for updates

Ag_2S Quantum Dots

How to cite:
International Edition: doi.org/10.1002/anie.202300085
German Edition: doi.org/10.1002/ange.202300085

Peptide-mediated Aqueous Synthesis of NIR-II Emitting Ag_2S Quantum Dots for Rapid Photocatalytic Bacteria Disinfection

Peiqing Sun, Kunlun Li, Xiao Liu, Jing Wang, Xusheng Qiu, Wei Wei,* and Jing Zhao**

Abstract: Pathogenic microorganisms in the environment are a great threat to global human health. The development of disinfection method with rapid and effective antibacterial properties is urgently needed. In this study, a biomimetic silver binding peptide AgBP2 was introduced to develop a facile synthesis of biocompatible Ag_2S quantum dots (QDs). The AgBP2 capped Ag_2S QDs exhibited excellent fluorescent emission in the second near-infrared (NIR-II) window, with physical stability and photostability in the aqueous phase. Under 808 nm NIR laser irradiation, AgBP2-Ag_2S QDs can serve not only as a photothermal agent to realize NIR photothermal conversion but also as a photocatalyst to generate reactive oxygen species (ROS). The obtained AgBP2-Ag_2S QDs achieved a highly effective disinfection efficacy of 99.06 % against *Escherichia coli* within 25 min of NIR irradiation, which was ascribed to the synergistic effects of photogenerated ROS during photocatalysis and hyperthermia. Our work demonstrated a promising strategy for efficient bacterial disinfection.

Introduction

Pathogenic bacteria in water sources pose a serious threat to healthcare due to their ability to cause bacterial infectious diseases.[1] Traditional bacterial disinfection methods such as ultraviolet (UV) light, chlorination, and ozone have been widely used in recent decades. Despite their widespread applications, these methods have several serious drawbacks, including high costs, low efficiency, poor biocompatibility, and carcinogenic by-products.[2] Therefore, it is highly desirable to develop rapid and energy-efficient water disinfection methods.

In recent years, nanomaterials with photothermal properties based on near-infrared (NIR) light irradiation have shown excellent potential in water disinfection.[3] To date, a series of photothermal nanomaterials with excellent performance, such as carbon-based materials,[2c,4] metal sulfides,[5] and magnetic nanoparticles,[6] have been developed. Among them, Ag_2S quantum dots (QDs) with photodynamic therapy (PDT) and photothermal therapy (PTT) properties have demonstrated excellent potential for biomedical applications due to their excellent NIR fluorescence properties and biocompatibility.[7] Ag_2S QDs act not only as NIR-II contrast agents but also as fluorescent nanothermometers.[8] Wang and colleagues first reported the fabrication of NIR-II fluorescent Ag_2S QDs by a single precursor source in 2010.[9] Subsequently, they made a series of important advances in the chemical synthesis and biomedical application of NIR Ag_2S QDs, showing great potential for bio-applications in biosensing, bioimaging, and theranostics.[10] However, few studies have been done to explore the application of Ag_2S QDs in water disinfection. Moreover, as-prepared Ag_2S QDs are usually synthesized under reaction conditions that require a complicated process and expensive reagents, which may greatly restrict their practical applications.[11]

Recently, a wide range of biomolecules, including DNA,[12] peptides,[13] and proteins,[14] have been reported for fabricating multifunctional nanomaterials under mild conditions.[15] Among them, Fan and co-workers elegantly used DNA origami templates to assemble silica-DNA composites with controlled sizes and shapes.[16] In addition, Gang et al. demonstrated that bifunctional comb-branched peptoids as stabilizing agents can effectively stabilize Au nanoparticles in ionic aqueous solutions.[17] These findings provide important guidance for aqueous synthesis of nanostructured materials. Inspired by these pioneering studies, in this work, biocompatible AgBP2-Ag_2S QDs were successfully synthesized using a silver binding peptide (AgBP2) as a template for bacterial disinfection under NIR light irradiation. The synthesized AgBP2-Ag_2S QDs showed high

[*] P. Sun, J. Wang, Prof. J. Zhao
State Key Laboratory of Coordination Chemistry, Chemistry and Biomedicine Innovation Center (ChemBIC), School of Chemistry and Chemical Engineering, Nanjing University
Nanjing 210023 (China)
E-mail: jingzhao@nju.edu.cn

K. Li, X. Liu, Prof. W. Wei
School of Life Sciences, Nanjing University
Nanjing 210023 (China)
E-mail: weiwei@nju.edu.cn

P. Sun, Prof. W. Wei, Prof. J. Zhao
Shenzhen Research Institute, Nanjing University
Shenzhen 518000 (China)
and
Nanchuang (Jiangsu) Institute of Chemistry and Health
Nanjing 210023 (China)

Dr. X. Qiu
Department of Orthopedics, Nanjing Drum Tower Hospital, The Affiliated Hospital of Nanjing University Medical School
Nanjing 210023 (China)
E-mail: qiu_xusheng@163.com

© 2023 Wiley-VCH GmbH

15213773, 0, Downloaded from https://onlinelibrary.wiley.com/doi/10.1002/anie.202300085 by Nanjing University, Wiley Online Library on [19/03/2023]. See the Terms and Conditions (https://onlinelibrary.wiley.com/terms-and-conditions) on Wiley Online Library for rules of use; OA articles are governed by the applicable Creative Commons License

photostability in different buffers. As expected, the AgBP2-Ag_2S QDs exhibited high photothermocatalytic disinfection of *E. coli* triggered by NIR light. On the basis of characterization and mechanistic analysis, the outstanding disinfection efficacy of AgBP2-Ag_2S QDs was attributed mainly to synergistic photothermal catalysis.

Results and Discussion

In the aqueous synthesis route, various biomolecules have been widely used to synthesize inorganic nanomaterials as stabilizers.[18] Due to their bioactive surfaces, biomolecule-conjugated nanomaterials are better suited for further biological applications.[19] Inspired by the study of Traxler and colleagues,[20] we realized that silver-binding peptides might perform a similar function as a stabilizer to promote the formation of Ag_2S QDs. Herein, we selected a silver-binding peptide (AgBP2) from a combinatorial display peptide library to prepare fluorescent Ag_2S QDs in an aqueous-phase solution. According to previously reported methods with modification, as shown in Figure 1a, the synthesis of AgBP2-Ag_2S QDs was initiated by incubating AgBP2 with $AgNO_3$ at room temperature to allow the binding of Ag^+ to AgBP2. The Na_2S solution was then quickly added to the AgBP2-Ag^+ complex with violent agitation to facilitate nanocrystal growth. A homogeneous brown solution was then obtained within several minutes under alkaline conditions, preliminarily indicating the formation of AgBP2-Ag_2S QDs. Through optimization, a molar ratio of Ag/S of 2:1 was selected, and the particles formed with other molar ratios exhibited no fluorescence property. The transmission electron microscopy (TEM) images showed that the synthesized AgBP2-Ag_2S QDs were monodisperse with an average size of less than 10 nm in aqueous solutions (Figure 1b), which was also observed in previous literature.[9] The high-resolution TEM results showed that the interplanar spacing of AgBP2-Ag_2S QD lattice fringes was 0.28 nm, which was assigned to the (−112) facets of monoclinic Ag_2S QDs (Figure 1c).[21] The energy-dispersive X-ray (EDX) spectroscopy with high-angle annular dark-field scanning transmission electron microscopy (HAADF-STEM) results clearly indicated that AgBP2-Ag_2S QDs were composed of Ag and S, and the Ag:S atomic ratio obtained from the EDX analysis was 1.87:1, which was close to the stoichiometry of Ag_2S (Figure 1d–i).

To further investigate the chemical characteristics of the synthesized AgBP2-Ag_2S QDs, X-ray photoelectron spectroscopy (XPS) was performed (Figure 2a). XPS peaks of 367.61 eV and 373.34 eV were corresponding to Ag $3d_{5/2}$ and $3d_{3/2}$ (Figure 2b), indicating that the silver oxidation state was monovalent in the AgBP2-Ag_2S QDs. The peak at 161.37 eV was the characteristic signal of S $2p_{3/2}$, which was in accordance with Ag–S bonds. The binding energy at 168.40 eV was corresponding to oxidized S, which may be the sample aged (Figure 2c). In addition, UV-visible (UV/Vis) absorption and photoluminescence (PL) spectra were obtained to measure the optical properties of the obtained AgBP2-Ag_2S QDs. As shown in Figure 2d, the absorption spectra of AgBP2-Ag_2S QDs were featureless with no discrete absorption features, which was ascribed to the unique electronic properties of Ag_2S QDs.[22] The PL spectrum presented an emission peak centred at 1072 nm in the second near-infrared window (NIR-II, 1000–1700 nm) upon illumination by an 808 nm laser, indicating the PL brightness nature of AgBP2-Ag_2S QDs (Figure 2e), which was consistent with previous reports.[21] The much narrower full width at half-maximum (FWHM) of the prepared AgBP2-Ag_2S QDs compared with previous reports[7d,22b] indicated a relatively narrow size distribution (Figure S1). Furthermore, the photophysical properties of AgBP2-Ag_2S QDs were also characterized (Figure S2). The fluorescence quantum yield was 2.07 % and the lifetime was 78 ns, which is preferable to most of Ag_2S QDs synthesized by small molecules, such as mercaptopropionic acid (MPA),[23] glutathione (GSH),[24] and polyethylene glycol (PEG)[25] (see the comparative graph Figure S3). This could be attributed to dots-medium energy transfer via non-radiative pathways reduced with the AgBP2 peptide-specific binding to Ag_2S QDs. The above results confirmed that AgBP2-Ag_2S QDs with NIR-II fluorescence were successfully synthesized in an aqueous solution.

The photostability and physical stability of photocatalysts are essential to photocatalytic performance.[28] To prepare AgBP2-Ag_2S QDs with better suitability for photocatalytic applications, the photostability of AgBP2-Ag_2S QDs was investigated. A photobleaching experiment was performed (Figure 2f). As a control, indocyanine green (ICG) was completely photobleached after NIR irradiation for 100 min, whereas AgBP2-Ag_2S QDs retained 97 % of its fluorescence. In addition, the colloidal stability of AgBP2-Ag_2S QDs in PBS, HEPES, and mediums was observed. As shown in Figure 2g, the AgBP2-Ag_2S QDs can be stably dispersed in different buffers without precipitation or aggregation, and no obvious change in the fluorescence was observed (Figure 2h), which may be due to the silver-binding peptide AgBP2 capped on its surface. Moreover, AgBP2-Ag_2S QDs added with different metal ions also exhibited no significant fluorescence changes (Figure 2i). Likewise, only a slight decrease in the fluorescence lifetime could be observed (Figure S4). We attributed this to the AgBP2 peptide-specific binding for silver ions[29] and the ultralow solubility product constant of Ag_2S QDs ($K_{sp} = 6.3 \times 10^{-50}$).[30] The above results indicated the excellent colloidal stability and photostability of NIR-II-emitting AgBP2-Ag_2S QDs, which is important for photocatalytic applications as photocatalysts.

To demonstrate the photothermal capabilities of AgBP2-Ag_2S QDs, the temperature changes of different concentrations of AgBP2-Ag_2S QDs were measured by recording the temperature during 808 nm laser irradiation (1.5 $W\,cm^{-2}$). As shown in Figure 3a, compared to that of the control group (PBS only), the temperature of AgBP2-Ag_2S QDs with different concentrations (50–300 $\mu g\,mL^{-1}$) increased by 22.1–58.6 °C after 6 min of NIR irradiation, indicating that the temperature increase of the AgBP2-Ag_2S QDs was concentration-dependent. Moreover, by fixing the concentration of the AgBP2-Ag_2S QDs (200 $\mu g\,mL^{-1}$), the

© 2023 Wiley-VCH GmbH

15213773, 0, Downloaded from https://onlinelibrary.wiley.com/doi/10.1002/anie.202300085 by Nanjing University, Wiley Online Library on [19/03/2023]. See the Terms and Conditions (https://onlinelibrary.wiley.com/terms-and-conditions) on Wiley Online Library for rules of use; OA articles are governed by the applicable Creative Commons License

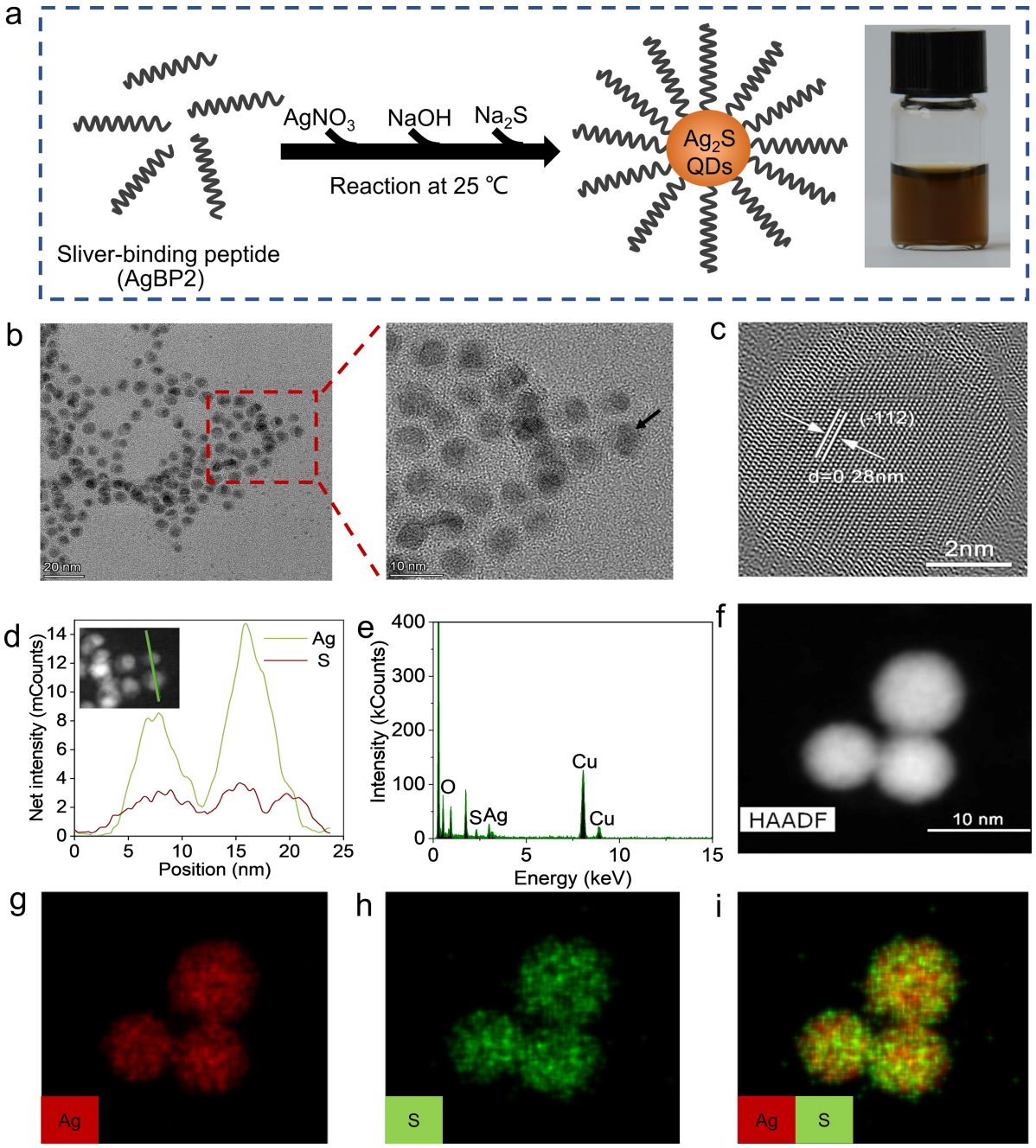

Figure 1. a) Schematic illustration of the aqueous-phase synthesis of fluorescent AgBP2-Ag_2S QDs. AgBP2: peptide sequence (EQLGVRKELRGV). Inset: Daylight image of the synthesized AgBP2-Ag_2S QDs. b) TEM and c) HRTEM images of AgBP2-Ag_2S QDs. d) Ag and S elemental profiles of AgBP2-Ag_2S QDs. The elemental profiles in (d) were obtained from EDX analysis (e) along the green line across AgBP2-Ag_2S QDs (inset of d). The EDX analysis in (e) was performed on the AgBP2-Ag_2S QDs indicated by the arrow in (b). f) HAADF-STEM images of AgBP2-Ag_2S QDs. g)–i) Element mappings of AgBP2-Ag_2S QDs.

temperature increased in a power-dependent manner (Figure 3b). With the concentration- and power-dependent photothermal properties, the final temperature of the AgBP2-Ag_2S QDs could be controlled under different conditions, which is extremely significant for killing bacteria at moderate temperatures. The heating/cooling curves of the AgBP2-Ag_2S QDs were shown in Figure 3c; there were almost no change after four cycles, suggesting that the AgBP2-Ag_2S QDs had an excellent photostability. We also measured the luminescent properties of AgBP2-Ag_2S QDs vary with temperature. Figure S5a showed the emission spectra as obtained from a colloidal dispersion of AgBP2-Ag_2S QDs obtained under 808 nm irradiation for temperatures ranging between 25 °C and 46 °C. Compared to the strong fluorescence quenching (90 % decrease) that happened in this temperature range,[31] a slight but not

© 2023 Wiley-VCH GmbH

15213773, 0, Downloaded from https://onlinelibrary.wiley.com/doi/10.1002/anie.202300085 by Nanjing University, Wiley Online Library on [19/03/2023]. See the Terms and Conditions (https://onlinelibrary.wiley.com/terms-and-conditions) on Wiley Online Library for rules of use; OA articles are governed by the applicable Creative Commons License

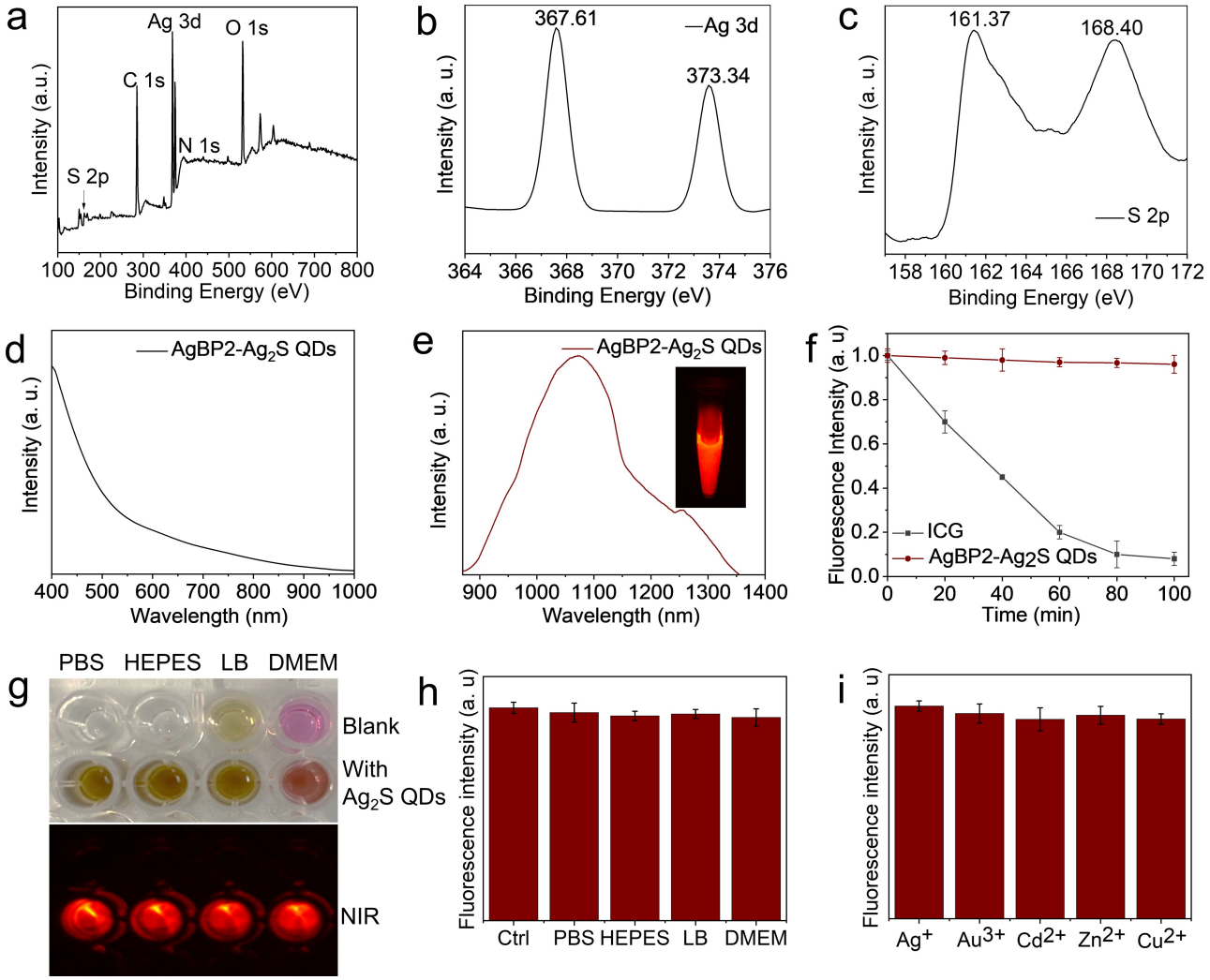

Figure 2. a) XPS survey spectrum of AgBP2-Ag_2S QDs and high-resolution b) Ag 3d and c) S 2p XPS spectra of the obtained AgBP2-Ag_2S QDs. d) UV-vis absorbance spectra and e) PL emission spectra of the as-prepared AgBP2-Ag_2S QDs under excitation with an 808 nm laser. Inset: NIR-II fluorescence image. f) Fluorescence stability of AgBP2-Ag_2S QDs and ICG after 100 min of irradiation with an 808 nm laser at 1.5 $W cm^{-2}$. g) Optical (up) and NIR-II fluorescence (down) images of colloidal dispersions of AgBP2-Ag_2S QDs (200 $\mu g mL^{-1}$) in PBS buffer (pH 7.4), 20 mM HEPES, Luria-Bertani (LB) medium (Difco™, Becton Dickinson, USA), and DMEM medium (Dulbecco's modified Eagle's medium, Gibco, New York, USA).[26] h) NIR-II fluorescence intensity of AgBP2-Ag_2S QDs in different buffers obtained from (g). i) NIR-II fluorescence intensity of AgBP2-Ag_2S QDs (200 $\mu g mL^{-1}$) with a final concentration of 1 mM Au^{3+}, Cd^{2+}, Zn^{2+}, and Cu^{2+}.[27] The error bars in (h) and (i) are from triplicate experiments.

significant decrease was observed (15% decrease), which was also identified in the fluorescence decay curves of the AgBP2-Ag_2S QDs at 25 °C and 46 °C (Figure S5b). These results indicated that the AgBP2-Ag_2S QDs had excellent photothermal stability. The photothermal conversion efficiency was also assessed. The photothermal conversion efficiency of AgBP2-Ag_2S QDs was calculated to be 63% (Figure 3d and e), which is significantly higher than that of different photothermal agents (e.g., ICG 3.1%,[32] Au nanorods 21%,[33] and Nano-BFF 28.6%[34]). Due to their outstanding photothermal-conversion ability, AgBP2-Ag_2S QDs have the potential to serve as photothermal reagents under NIR irradiation. In addition, the final temperature of the AgBP2-Ag_2S QDs at a concentration of 200 $\mu g mL^{-1}$ reached 50 °C after irradiation with an 808 nm laser at a density of 1.5 $W cm^{-2}$ (Figure 3f and g), which is sufficient to kill bacteria. Thus, the concentration of the AgBP2-Ag_2S QDs (200 $\mu g mL^{-1}$) was selected for subsequent antibacterial testing under NIR light irradiation (1.5 $W cm^{-2}$). Additionally, the gram-negative bacterium *E. coli* k-12 was used as the bacterial model for all experiments.

The toxicity caused by AgBP2-Ag_2S QDs is an important factor affecting photothermal disinfection performance. The optical density of *E. coli* at 600 nm (OD_{600}) was recorded. As shown in Figure S6, compared to that of the positive control group (*E. coli* only), the OD_{600} value of *E. coli* treated with AgBP2-Ag_2S QDs gradually increased to 2.02 at 37.0 °C in the dark overnight, suggesting that the AgBP2-Ag_2S QDs had almost no toxic effect on bacterial growth. The spread plate method was used to investigate the

© 2023 Wiley-VCH GmbH

15213773, 0, Downloaded from https://onlinelibrary.wiley.com/doi/10.1002/anie.202300085 by Nanjing University, Wiley Online Library on [19/03/2023]. See the Terms and Conditions (https://onlinelibrary.wiley.com/terms-and-conditions) on Wiley Online Library for rules of use; OA articles are governed by the applicable Creative Commons License

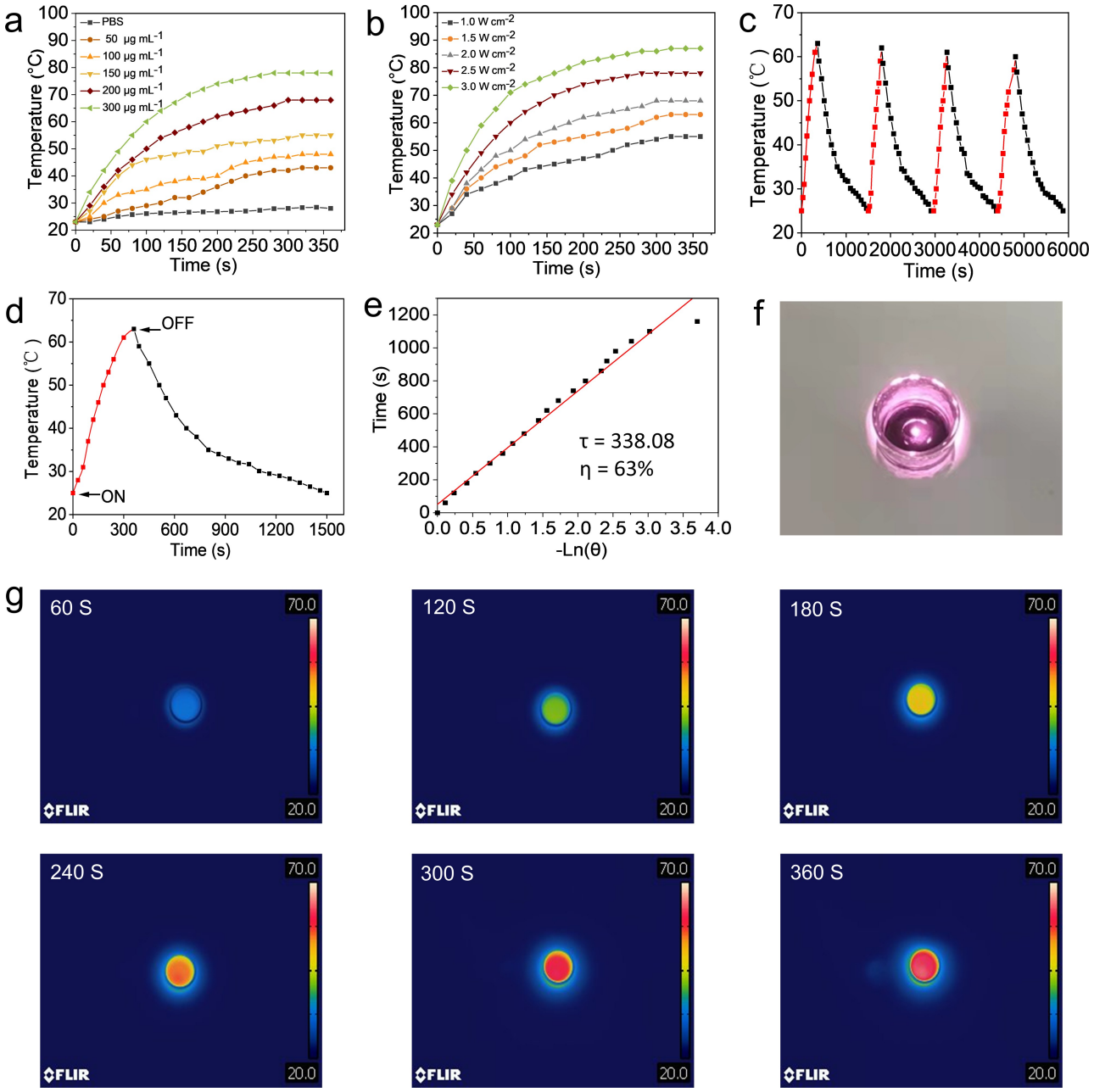

Figure 3. a) Temperature elevations of the AgBP2-Ag_2S QDs at different concentrations (808 nm, 1.5 W cm^{-2}) and at different powers under 6 min irradiation (808 nm, 200 μg mL^{-1}) (b). c) The heating-cooling curve of the AgBP2-Ag_2S QDs for four cycles under NIR irradiation (1.5 W cm^{-2}). d) Photothermal performance of the AgBP2-Ag_2S QDs under NIR irradiation (1.5 W cm^{-2}) for 6 min, and the laser was turned off. e) The Linear fitting curve between time and $-\mathrm{Ln}(\theta)$ acquired from the cooling process. f) Daylight images. g) Photothermal imaging of AgBP2-Ag_2S QDs for various durations in 6 minutes.

disinfection efficacy of the AgBP2-Ag_2S QDs against *E. coli* under NIR irradiation. In the reaction system, the cell density was adjusted to a final value of 1.5×10^7 CFU (colony forming unit)/mL. As depicted in Figure 4, compared to the control group (dark), almost all the *E. coli* colonies without AgBP2-Ag_2S QDs survived after NIR irradiation for 25 min. In contrast, *E. coli* colonies treated with AgBP2-Ag_2S QDs exhibited evident disinfection efficacy under the same conditions (Figure 4a), with a disinfection percentage of 99.06 % (Figure 4b). In addition to colony counting and growth behavior, cell membrane integrity is also an index of cell survival. A live/dead staining assay was performed based on SYTO 9/propidium iodide (PI) staining. PI, a red-fluorescent dye, can only penetrate damaged walls of bacteria, while SYTO 9, a green fluorescent dye, marks live bacteria that have a complete cell membrane.[35] As shown in Figure 4c, no red fluorescence was detected in the control group (dark). However, a strong red fluorescent dot was clearly visible in *E. coli* treated with AgBP2-Ag_2S QDs and NIR irradiation, indicating the destruction of the cell walls.

© 2023 Wiley-VCH GmbH

15213773, 0, Downloaded from https://onlinelibrary.wiley.com/doi/10.1002/anie.202300085 by Nanjing University, Wiley Online Library on [19/03/2023]. See the Terms and Conditions (https://onlinelibrary.wiley.com/terms-and-conditions) on Wiley Online Library for rules of use; OA articles are governed by the applicable Creative Commons License

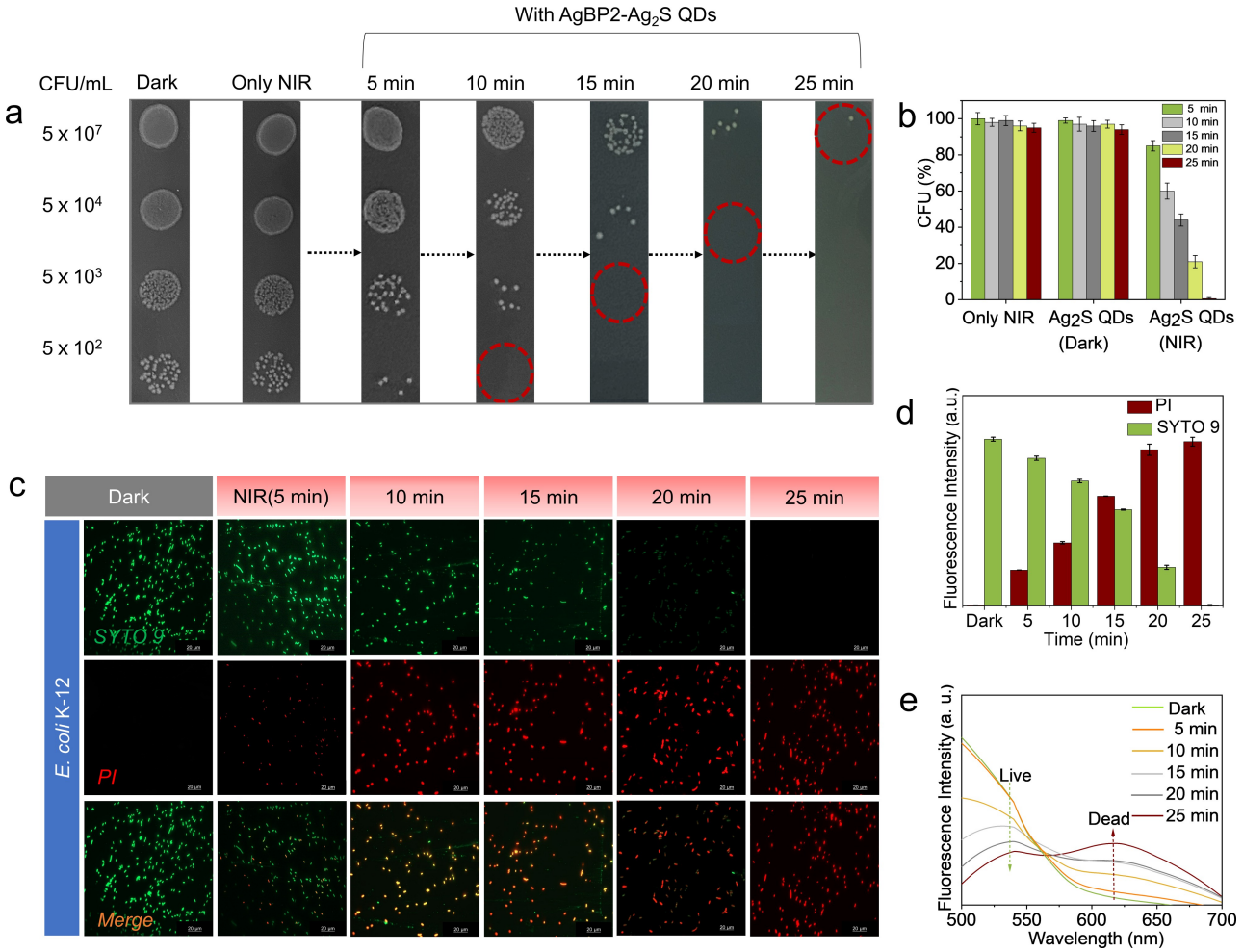

Figure 4. a) Photographs of bacterial colonies in the plate-sensitivity assay. All plates were incubated at 37 °C for 16 h after different treatments. b) CFU ratios of *E. coli* colonies in the spread-plate assay after being treated with NIR, AgBP2-Ag_2S QDs + dark, and AgBP2-Ag_2S QDs + NIR. c) Live/dead staining images of *E. coli* costained with SYTO 9 (green) and PI (red) after being treated with AgBP2-Ag_2S QDs with or without 808 nm NIR illumination. Scale bars: 20 μm. d) Fluorescence intensity of *E. coli* costained with SYTO 9 (excitation/emission maxima are at 480 nm/500 nm) and PI (excitation/emission maxima are at 490 nm/635 nm). e) The resulting fluorescence emission spectrum was measured with 470 nm excitation from (c). The error bars in (b) and (d) are from triplicate experiments.

Similar results can be seen in Figure 4d and Figure 4e. These results were consistent with the results of the spread plate method. Additionally, we also added the same size of GSH-Ag_2S QDs as a control and measured the disinfection performance of GSH-Ag_2S QDs. As shown in Figure S7, the cell density only decreased to 6.53 log10 CFU mL^{-1}, implying a lower catalytic efficiency than that of AgBP2-Ag_2S QDs. All these abovementioned results clearly indicated that AgBP2-Ag_2S QDs with high photothermal conversion efficiency could be used for photothermal disinfection.

To elucidate the synergistic effect of photothermal catalysis on bacterial disinfection, a series of control experiments were performed, and the results are illustrated in Figure 5. As shown in Figure 5a, the cell density exhibited no obvious decrease in the control groups (light and dark control) within 25 min, indicating that the influence of light intensity and the photocatalyst on bacterial growth could be neglected. In contrast, after adding AgBP2-Ag_2S QDs to the system under NIR irradiation, the cell density decreased from 7.1 log10 to 0. Next, to investigate the contribution of hyperthermia in the disinfection process, the disinfection efficiency at high temperature was measured. Compared with the control group (AgBP2-Ag_2S QDs + 37 °C), the disinfection efficiencies of AgBP2-Ag_2S QDs + 46 °C, AgBP2-Ag_2S QDs + NIR (25 °C), and AgBP2-Ag_2S QDs + NIR groups reached 36.54 %, 59.41 % and 99.06 %, respectively (Figure 5b and c). The above results clearly indicated that only ROS or hyperthermia alone was not strong enough for lethal killing *E. coli.* Whereas, after the combination treatment of hyperthermia and ROS, the AgBP2-Ag_2S QD_S + NIR group effectively killed most of *E. coli.* In addition, the combination index (CI) was further determined to evaluate whether the inhibition of *E. coli* effects was additive or synergistic.[36] As shown in Figure S8, the calculated combination index for the AgBP2-Ag_2S QDS + (NIR) group was CI < 1, which is characteristic for synergism.[37] The pseudo-first-order kinetic rate constant k related to photothermal synergy was the highest (0.11 min^{-1})

© 2023 Wiley-VCH GmbH

15213773, 0, Downloaded from https://onlinelibrary.wiley.com/doi/10.1002/anie.202300085 by Nanjing University, Wiley Online Library on [19/03/2023]. See the Terms and Conditions (https://onlinelibrary.wiley.com/terms-and-conditions) on Wiley Online Library for rules of use; OA articles are governed by the applicable Creative Commons License

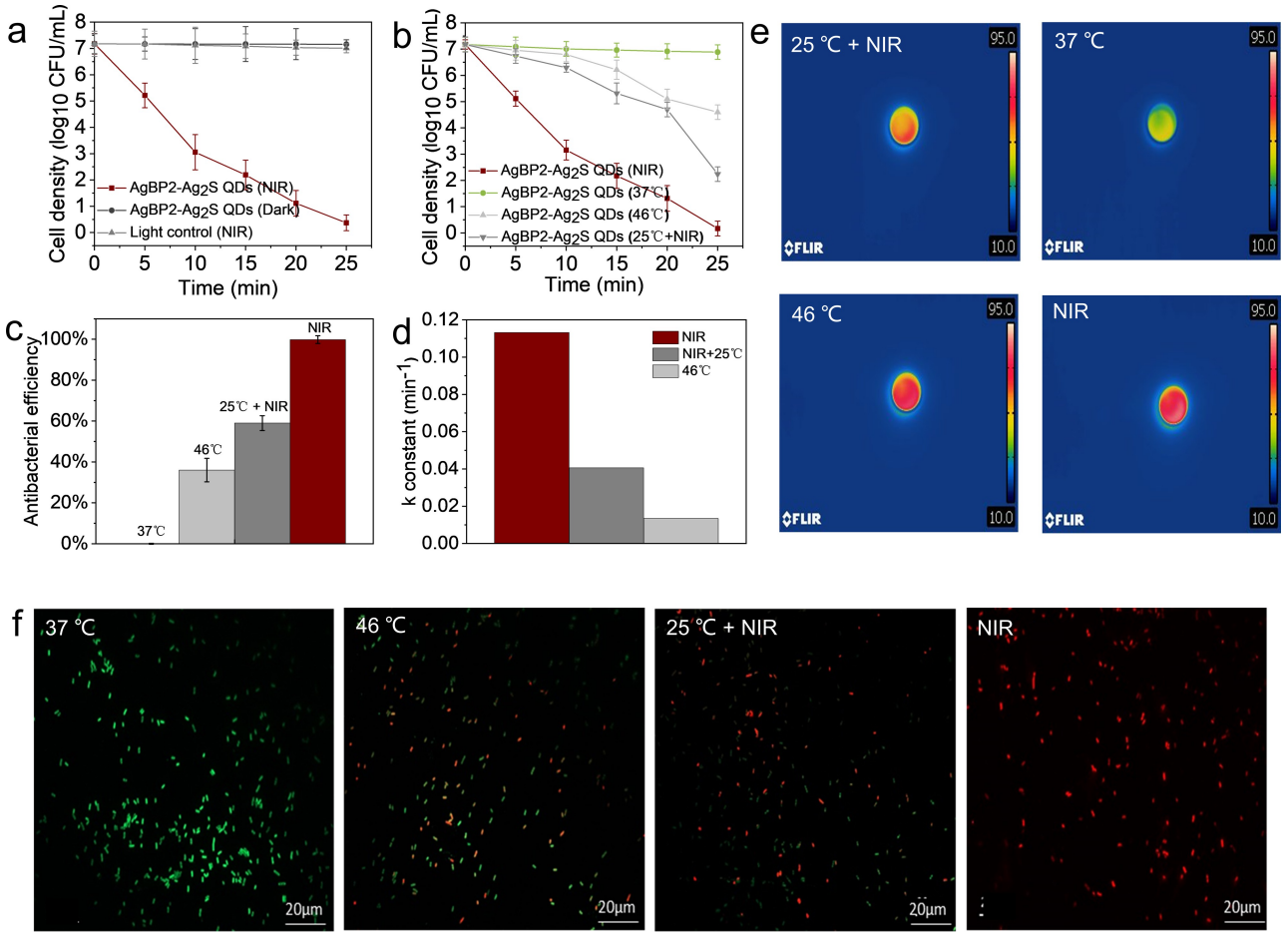

Figure 5. a), b) Disinfection performance of AgBP2-Ag_2S QDs against *E. coli* (1.5×10^7 CFU mL^{-1}) under different conditions. c) Relative bacterial viabilities of *E. coli* calculated by CFU counting. d) The reaction rate constant (*k*) of the bactericidal dynamics curves. e) Photothermal imaging of the bacterial solution after different treatments. f) Live/dead staining images of *E. coli* after different treatments with AgBP2-Ag_2S QDs (200 μg mL^{-1}) with or without NIR irradiation (1.5 W cm^{-2}, 25 min). The error bars in (a–c) are from triplicate experiments.

(Figure 5d), indicating a higher efficiency than that of photocatalysis and thermal catalysis (Figure S9). Similar results were obtained in the spread plate assay (Figure S10) and the live/dead fluorescent staining test (Figures S11 and S12).

The production of reactive oxygen species (ROS) has been recognized as a critical step in explaining bacterial disinfection during photocatalysis.[38] To investigate the generation of ROS and their contribution to the photocatalytic disinfection process, various kinds of scavengers were added to the reaction system. The concentration of the scavengers was optimized to ensure no toxic effect on *E. coli* cells within 25 min (Figure S13). Specifically, TEMPOL, $Na_2C_2O_4$, and isopropanol (IPA) were selected as scavengers of $^{\bullet}O_2^-$, holes (h^+), and $^{\bullet}OH$, respectively.[39] As depicted in Figure 6a, compared to that of the control group (no scavenger), the cell density of *E. coli* decreased to 1.54 log10 CFU mL^{-1} and 0.95 log10 CFU mL^{-1} after the addition of TEMPOL and $Na_2C_2O_4$, respectively, suggesting that $^{\bullet}O_2^-$ and h^+ are the dominant reactive species in the disinfection process. However, after adding IPA to the system, the cell density remained almost unchanged, suggesting that $^{\bullet}OH$ was not involved in the photocatalytic process. To further verify the reactive oxygen radicals generated from AgBP2-Ag_2S QDs under NIR irradiation, the ESR test was performed to confirm the presence of active radicals by using 5,5-dimethyl-1-pyrroline N-oxide (DMPO) as a spin-trapping reagent. As shown in Figure 6b, no apparent $^{\bullet}O_2^-$ signal was observed in the ESR spectrum under dark conditions, while the characteristic peaks (1:1:1:1) of $^{\bullet}O_2^-$ were detected and became gradually more intense over time, further suggesting that the generation of $^{\bullet}O_2^-$ during NIR irradiation. In contrast, the characteristic peaks of DMPO/·OH (1:2:2:1) adducts were not observed under the same conditions (Figure S14). In addition, based on the UV-vis diffuse reflectance spectroscopy (UV/Vis DRS) and the corresponding experimental Tauc plot of AgBP2-Ag_2S QDs (Figure S15), the band gap of AgBP2-Ag_2S QDs was about 1.86 eV. Meanwhile, the potential values of the conduction band (CB) and valence band (VB) of AgBP2-Ag_2S QDs can be calculated according to the equations.[40] The calculated CB and VB potential of AgBP2-Ag_2S QDs were −0.47 eV and 1.39 eV, respectively. Under NIR irradiation, AgBP2-Ag_2S QDs could be excited to generate the electron-hole

© 2023 Wiley-VCH GmbH

15213773, 0, Downloaded from https://onlinelibrary.wiley.com/doi/10.1002/anie.202300085 by Nanjing University, Wiley Online Library on [19/03/2023]. See the Terms and Conditions (https://onlinelibrary.wiley.com/terms-and-conditions) on Wiley Online Library for rules of use; OA articles are governed by the applicable Creative Commons License

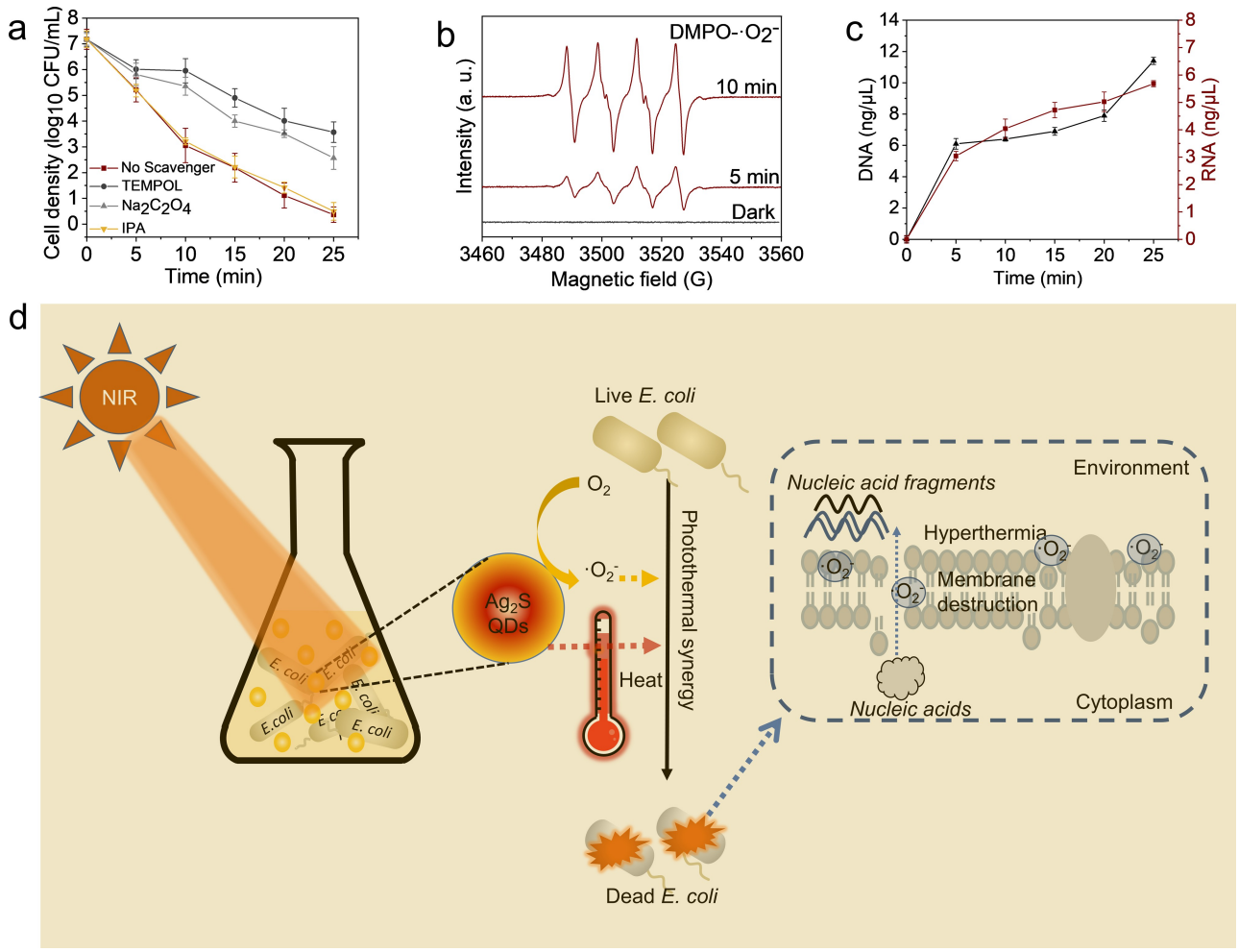

Figure 6. a) Photocatalytic disinfection efficiency against *E. coli* upon the addition of different scavengers (1 mM TEMPOL, 7.5 mM isopropanol, and 0.5 mM $Na_2C_2O_4$). b) ESR spectra of DMPO/$^{\bullet}O_2^-$ in the presence of AgBP2-Ag_2S QDs under 808 nm light irradiation. c) The real-time concentration of DNA and RNA released during bacterial cell destruction. d) Disinfection mechanism of AgBP2-Ag_2S QDs under NIR irradiation. The error bars in (a) and (c) are from triplicate experiments.

pairs. Due to the potential of $O_2/^{\bullet}O^{2-}$ (−0.28 eV vs. NHE), the activated electrons reacted with the surface-absorbed O_2 to generate $^{\bullet}O^{2-}$. However, as the potential of $^{\bullet}OH/H_2O$ (2.38 eV vs. NHE) was lower than the VB of AgBP2-Ag_2S QDs (1.39 eV vs. NHE), oxidative species ($^{\bullet}OH$) cannot be generated, which was consistent with ESR results. Moreover, we measured the variations in the absorption spectrum of AgBP2-Ag_2S QDs during the disinfection experiment. As shown in Figure S16, an obvious decrease of AgBP2-Ag_2S QDs absorption was concomitantly observed, corresponding to a decline in disinfection performance (Figure 5a), which was attributed to AgBP2-Ag_2S QDs oxidation caused by H_2O_2. To better understand the bacterial disinfection process, a detailed study of cell destruction was carried out. The leakage of DNA and RNA contents was investigated to determine the degree of bacterial destruction. Nanodrop was used to measure the concentrations of DNA and RNA, and the results indicated that an increasing amount of nucleic acids was released into the suspension during the disinfection process (Figure 6c). The results suggested that the reactive species disrupted the bacterial cells, ultimately causing the nucleic acids inside the dead cells to leak out. Moreover, the disinfection efficacy shown in Figure S17 further indicated that the synergy of ROS and photothermal effect achieved much better disinfection performance than single ROS or photothermal effect alone. Therefore, the excellent disinfection performance can be attributed to the synergistic results of NIR-induced ROS and photothermal effect. The cell viability results showed that AgBP2-Ag_2S QDs was not cytotoxic, and that only a relatively short irradiation time could decrease cellular proliferation (Figure S18).

On the basis of the abovementioned results, a synergistic photothermal disinfection mechanism of AgBP2-Ag_2S QDs for *E. coli* under NIR irradiation was proposed, as shown in Figure 6d. Highly efficient photocatalytic disinfection of *E. coli* was achieved over AgBP2-Ag_2S QDs during NIR irradiation. The interaction of photogenerated ROS ($^{\bullet}O_2^-$ and h^+) with *E. coli* can damage the structure of cell membranes and the leakage of nucleic acids inside cells,

© 2023 Wiley-VCH GmbH

15213773, 0, Downloaded from https://onlinelibrary.wiley.com/doi/10.1002/anie.202300085 by Nanjing University, Wiley Online Library on [19/03/2023]. See the Terms and Conditions (https://onlinelibrary.wiley.com/terms-and-conditions) on Wiley Online Library for rules of use; OA articles are governed by the applicable Creative Commons License

ultimately leading to bacterial death. In addition, the AgBP2-Ag_2S QDs possessed excellent photothermal conversion efficiency, which could further accelerate the disinfection performance during photocatalysis. Overall, the synergistic effects of photocatalytic and photothermal catalysis substantially improved the disinfection performance of AgBP2-Ag_2S QDs.

Conclusion

In summary, AgBP2-Ag_2S QDs were successfully synthesized in the aqueous phase based on a silver-binding polypeptide and served as photothermal agents for disinfection activity. The synthesized AgBP2-Ag_2S QDs with NIR-II fluorescence exhibited excellent photostability and photothermal effects. The photogenerated ROS ($^{\bullet}O_2^-$ and h^+) from AgBP2-Ag_2S QDs were the dominant reactive species during photocatalytic disinfection. Owing to the strong synergy of ROS and photothermal effect, the AgBP2-Ag_2S QDs showed a disinfection efficacy of 99.06% against *E. coli* within 25 min of NIR irradiation. This research provides a new strategy for constructing high-performance photothermal agents for rapid disinfection.

Acknowledgements

Financial support was provided by the National Natural Science Foundation of China (22025701 and 22177048), Shenzhen Basic Research Program (JCYJ20180508182240106), and the Shenzhen Bay Laboratory Open Fund Project (SZBL2021080601013).

Conflict of Interest

The authors declare no conflict of interest.

Data Availability Statement

The data that support the findings of this study are available from the corresponding author upon reasonable request.

Keywords: Ag_2S QDs · Antibacterial · Aqueous Synthesis · Photothermal Synergy · Reactive Oxygen Species

[1] F. O. Nestle, P. Di Meglio, J. Z. Qin, B. J. Nickoloff, *Nat. Rev. Immunol.* **2009**, *9*, 679–691.
[2] a) B. Ezraty, A. Gennaris, F. Barras, J. F. Collet, *Nat. Rev. Microbiol.* **2017**, *15*, 385–396; b) R. M. Zhang, C. J. Song, M. P. Kou, P. Q. Yin, X. L. Jin, L. Wang, Y. Deng, B. Wang, D. H. Xia, P. K. Wong, L. Q. Ye, *Environ. Sci. Technol.* **2020**, *54*, 3691–3701; c) Z. Zhang, J. Y. Sun, X. Chen, G. Z. Wu, Z. G. Jin, D. G. Guo, L. Liu, *J. Hazard. Mater.* **2021**, *419*, 126462.
[3] a) M. A. Shannon, P. W. Bohn, M. Elimelech, J. G. Georgiadis, B. J. Marinas, A. M. Mayes, *Nature* **2008**, *452*, 301–310; b) D. H. Xia, H. D. Liu, B. H. Xu, Y. C. Wang, Y. H. Liao, Y. J. Huang, L. Q. Ye, C. He, P. K. Wong, R. L. Qiu, *Appl. Catal. B* **2019**, *245*, 177–189.
[4] a) Z. H. Qi, P. Bharate, C. H. Lai, B. Ziem, C. Bottcher, A. Schulz, F. Beckert, B. Hatting, R. Mulhaupt, P. H. Seeberger, R. Haag, *Nano Lett.* **2015**, *15*, 6051–6057; b) J. F. Li, Z. Y. Li, X. M. Liu, C. Y. Li, Y. F. Zheng, K. W. K. Yeung, Z. D. Cui, Y. Q. Liang, S. L. Zhu, W. B. Hu, Y. J. Qi, T. J. Zhang, X. B. Wang, S. L. Wu, *Nat. Commun.* **2021**, *12*, 1224.
[5] a) M. Zhu, X. M. Liu, L. Tan, Z. D. Cui, Y. Q. Liang, Z. Y. Li, K. W. K. Yeung, S. L. Wu, *J. Hazard. Mater.* **2020**, *383*, 121122; b) Y. F. Lin, D. L. Han, Y. Li, L. Tan, X. M. Liu, Z. D. Cui, X. J. Yang, Z. Y. Li, Y. Q. Liang, S. L. Zhu, S. L. Wu, *ACS Sustainable Chem. Eng.* **2019**, *7*, 14982–14990.
[6] a) T. J. Yu, P. H. Li, T. W. Tseng, Y. C. Chen, *Nanomedicine* **2011**, *6*, 1353–1363; b) D. H. Xia, H. J. W. He, H. D. Liu, Y. C. Wang, Q. Zhang, Y. Li, A. H. Lu, C. He, P. K. Wong, *Appl. Catal. B* **2018**, *238*, 70–81; c) B. Peng, X. L. Zhang, D. Aarts, R. P. A. Dullens, *Nat. Nanotechnol.* **2018**, *13*, 478–482.
[7] a) G. S. Hong, J. T. Robinson, Y. J. Zhang, S. Diao, A. L. Antaris, Q. B. Wang, H. J. Dai, *Angew. Chem. Int. Ed.* **2012**, *51*, 9818–9821; *Angew. Chem.* **2012**, *124*, 9956–9959; b) S. Chen, *Science* **2019**, *365*, 456–457; c) X. Michalet, F. F. Pinaud, L. A. Bentolila, J. M. Tsay, S. Doose, J. J. Li, G. Sundaresan, A. M. Wu, S. S. Gambhir, S. Weiss, *Science* **2005**, *307*, 538–544; d) P. Jiang, Z. Q. Tian, C. N. Zhu, Z. L. Zhang, D. W. Pang, *Chem. Mater.* **2012**, *24*, 3–5.
[8] Y. L. Shen, J. Lifante, E. Ximendes, H. D. A. Santos, D. Ruiz, B. H. Juarez, I. Z. Gutierrez, V. T. Vera, J. R. Retama, E. M. Rodriguez, D. H. Ortgies, D. Jaque, A. Benayas, B. del Rosal, *Nanoscale* **2019**, *11*, 19251–19264.
[9] Y. P. Du, B. Xu, T. Fu, M. Cai, F. Li, Y. Zhang, Q. B. Wang, *J. Am. Chem. Soc.* **2010**, *132*, 1470–1471.
[10] C. Li, G. Chen, Y. Zhang, F. Wu, Q. Wang, *J. Am. Chem. Soc.* **2020**, *142*, 14789–14804.
[11] Y. Zhang, H. Yang, X. An, Z. Wang, X. Yang, M. Yu, R. Zhang, Z. Sun, Q. Wang, *Small* **2020**, *16*, 2001003.
[12] M. Madsen, K. V. Gothelf, *Chem. Rev.* **2019**, *119*, 6384–6458.
[13] R. Lévy, N. T. K. Thanh, R. C. Doty, I. Hussain, R. J. Nichols, D. J. Schiffrin, M. Brust, D. G. Fernig, *J. Am. Chem. Soc.* **2004**, *126*, 10076–10084.
[14] R. Sanghi, P. Verma, *Bioresour. Technol.* **2009**, *100*, 501–504.
[15] a) B. P. Gray, K. C. Brown, *Chem. Rev.* **2014**, *114*, 1020–1081; b) Y. Ju, H. T. Liao, J. J. Richardson, J. L. Guo, F. Caruso, *Chem. Soc. Rev.* **2022**, *51*, 4287–4336.
[16] X. G. Liu, F. Zhang, X. X. Jing, M. C. Pan, P. Liu, W. Li, B. W. Zhu, J. Li, H. Chen, L. H. Wang, J. P. Lin, Y. Liu, D. Y. Zhao, H. Yan, C. H. Fan, *Nature* **2018**, *559*, 593–598.
[17] S. T. Wang, H. H. Zhang, S. T. Xuan, D. Nykypanchuk, Y. G. Zhang, G. Freychet, B. M. Ocko, R. N. Zuckermann, N. Todorova, O. Gang, *J. Am. Chem. Soc.* **2022**, *144*, 8138–8152.
[18] C. L. Chen, N. L. Rosi, *Angew. Chem. Int. Ed.* **2010**, *49*, 1924–1942; *Angew. Chem.* **2010**, *122*, 1968–1986.
[19] a) M. Naito, K. Iwahori, A. Miura, M. Yamane, I. Yamashita, *Angew. Chem. Int. Ed.* **2010**, *49*, 7006–7009; *Angew. Chem.* **2010**, *122*, 7160–7163; b) X. X. Wang, Z. C. Han, W. Wei, H. S. Hu, P. F. Li, P. Q. Sun, X. Z. Liu, Z. J. Lv, F. Wang, Y. Cao, Z. J. Guo, J. Li, J. Zhao, *Chem. Sci.* **2022**, *13*, 7269–7275.
[20] R. Hall Sedlak, M. Hnilova, C. Grosh, H. Fong, F. Baneyx, D. Schwartz, M. Sarikaya, C. Tamerler, B. Traxler, *Appl. Environ. Microbiol.* **2012**, *78*, 2289–2296.
[21] Y. Zhang, G. S. Hong, Y. J. Zhang, G. C. Chen, F. Li, H. J. Dai, Q. B. Wang, *ACS Nano* **2012**, *6*, 3695–3702.
[22] a) Y. J. Zhang, Y. S. Liu, C. Y. Li, X. Y. Chen, Q. B. Wang, *J. Phys. Chem. C* **2014**, *118*, 4918–4923; b) H. Y. Yang, Y. W. Zhao, Z. Y. Zhang, H. M. Xiong, S. N. Yu, *Nanotechnology* **2013**, *24*, 055706.

© 2023 Wiley-VCH GmbH

15213773, 0, Downloaded from https://onlinelibrary.wiley.com/doi/10.1002/anie.202300085 by Nanjing University, Wiley Online Library on [19/03/2023]. See the Terms and Conditions (https://onlinelibrary.wiley.com/terms-and-conditions) on Wiley Online Library for rules of use; OA articles are governed by the applicable Creative Commons License

[23] P. Jiang, C. N. Zhu, Z. L. Zhang, Z. Q. Tian, D. W. Pang, *Biomaterials* **2012**, *33*, 5130–5135.
[24] C. X. Wang, Y. Wang, L. Xu, D. Zhang, M. X. Liu, X. W. Li, H. C. Sun, Q. Lin, B. Yang, *Small* **2012**, *8*, 3137–3142.
[25] A. Paściak, R. Marin, L. Abiven, A. Pilch-Wrobel, M. Misiak, W. J. Xu, K. Prorok, O. Bezkrovnyi, L. Marciniak, C. Chaneac, F. Gazeau, R. Bazzi, S. Roux, B. Viana, V. P. Lehto, D. Jaque, A. Bednarkiewicz, *ACS Appl. Mater. Interfaces* **2022**, *14*, 33555–33566.
[26] Q. Wang, H. T. Yang, Q. Zhang, H. G. Ge, S. R. Zhang, Z. Y. Wang, X. H. Ji, *Microchim. Acta* **2019**, *186*, 468.
[27] W. Wei, T. Z. Zhu, Y. Wang, H. L. Yang, Z. Y. Hao, P. R. Chen, J. Zhao, *Chem. Sci.* **2012**, *3*, 1780–1784.
[28] U. I. Gaya, A. H. Abdullah, *J. Photochem. Photobiol. C* **2008**, *9*, 1–12.
[29] S. Eckhardt, P. S. Brunetto, J. Gagnon, M. Priebe, B. Giese, K. M. Fromm, *Chem. Rev.* **2013**, *113*, 4708–4754.
[30] R. J. Gui, H. Jin, Z. H. Wang, L. J. Tan, *Coord. Chem. Rev.* **2015**, *296*, 91–124.
[31] H. D. A. Santos, D. Ruiz, G. Lifante, C. Jacinto, B. H. Juarez, D. Jaque, *Nanoscale* **2017**, *9*, 2505–2513.
[32] H. S. Jung, J. H. Lee, K. Kim, S. Koo, P. Verwilst, J. L. Sessler, C. Kang, J. S. Kim, *J. Am. Chem. Soc.* **2017**, *139*, 9972–9978.
[33] J. Zeng, D. Goldfeld, Y. N. Xia, *Angew. Chem. Int. Ed.* **2013**, *52*, 4169–4173; *Angew. Chem.* **2013**, *125*, 4263–4267.
[34] H. J. Xiang, L. Z. Zhao, L. D. Yu, H. Z. Chen, C. Y. Wei, Y. Chen, Y. L. Zhao, *Nat. Commun.* **2021**, *12*, 218.
[35] J. Wang, F. Li, Z. Xu, M. Zang, S. Liu, T. Li, J. Xu, H. Sun, S. Yu, J. Liu, *Chem. Eng. J.* **2022**, *444*, 136620.
[36] T. C. Chou, P. Talalay, *Adv. Enzyme Regul.* **1984**, *22*, 27–55.
[37] T. C. Chou, *Pharm. Rev.* **2006**, *58*, 621–681.
[38] Y. Nosaka, A. Y. Nosaka, *Chem. Rev.* **2017**, *117*, 11302–11336.
[39] Z. Jiang, B. Wang, Y. Li, H. S. Chan, H. Sun, T. Wang, H. Li, S. Yuan, M. K. H. Leung, A. Lu, P. K. Wong, *Appl. Catal. B* **2019**, *257*, 117898.
[40] Q. Wu, M. Zhou, Y. Gong, Q. Li, M. Yang, Q. Yang, Z. Zhang, *Catal. Sci. Technol.* **2018**, *8*, 5225–5235.

Manuscript received: January 3, 2023
Accepted manuscript online: February 11, 2023
Version of record online: ■■, ■■

© 2023 Wiley-VCH GmbH

15213773, 0, Downloaded from https://onlinelibrary.wiley.com/doi/10.1002/anie.202300085 by Nanjing University, Wiley Online Library on [19/03/2023]. See the Terms and Conditions (https://onlinelibrary.wiley.com/terms-and-conditions) on Wiley Online Library for rules of use; OA articles are governed by the applicable Creative Commons License

Research Articles

Ag_2S Quantum Dots

P. Sun, K. Li, X. Liu, J. Wang, X. Qiu,*
W. Wei,* J. Zhao* e202300085

Peptide-mediated Aqueous Synthesis of NIR-II Emitting Ag_2S Quantum Dots for Rapid Photocatalytic Bacteria Disinfection

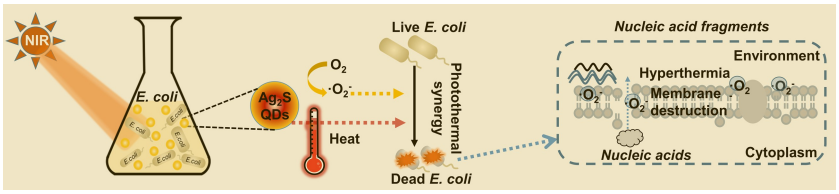

NIR-II-emitting AgBP2-Ag_2S QDs were successfully synthesized based on a silver-binding polypeptide AgBP2 under mild conditions and served as photothermal agents for antibacterial activity. Owing to the synergistic effects of photogenerated ROS and hyperthermia, the obtained AgBP2-Ag_2S QDs exhibited an effective disinfection efficacy of 99.06% against *E. coli* within 25 min of NIR irradiation.

© 2023 Wiley-VCH GmbH

15213773, 0, Downloaded from https://onlinelibrary.wiley.com/doi/10.1002/anie.202300085 by Nanjing University, Wiley Online Library on [19/03/2023]. See the Terms and Conditions (https://onlinelibrary.wiley.com/terms-and-conditions) on Wiley Online Library for rules of use; OA articles are governed by the applicable Creative Commons License